PNAS RESEARCH ARTICLE | CHEMISTRY

Single-crystal-to-single-crystal translation of a helical supramolecular polymer to a helical covalent polymer

Ravichandran Khazeber[a] and Kana M. Sureshan[a,1]

Edited by Lia Addadi, Weizmann Institute of Science, Rehovot, Israel; received March 29, 2022; accepted May 30, 2022

Polymers possessing helical conformation in the solid state are in high demand. We report a helical peptide-polymer via the topochemical ene-azide cycloaddition (TEAC) polymerization. The molecules of the designed Gly-Phe–based dipeptide, decorated with ene and azide, assemble in its crystals as β-sheets and as supramolecular helices in two mutually perpendicular directions. While the NH…O H-bonding facilitates β-sheet–like stacking along one direction, weak CH…N H-bonding between the azide-nitrogen and vinylic-hydrogen of molecules belonging to the adjacent stacks arranges them in a head-to-tail manner as supramolecular helices. In the crystal lattice, the azide and alkene of adjacent molecules in the supramolecular helix are suitably preorganized for their TEAC reaction. The dipeptide underwent regio- and stereospecific polymerization upon mild heating in a single-crystal-to-single-crystal fashion, yielding a triazoline-linked helical covalent polymer that could be characterized by single-crystal X-ray diffraction studies. Upon heating, the triazoline-linked polymer undergoes denitrogenation to aziridine-linked polymer, as evidenced by differential scanning calorimetry, thermogravimetric analysis, and solid-state NMR analyses.

helical polymers | crystal engineering | topochemical reaction | triazoline-linked polymer | supramolecular chemistry

Significance

Synthetic helical polymers have important applications in chiral chromatography, asymmetric catalysis, chiral recognition, optics, controlled release, circularly polarized luminescence, optical memory, spin filtering, and biomedical fields, among others. Many of these applications necessitate the helicity in the solid form of these polymers. However, the conventional solution-synthesized helical polymers often lose their helicity during desolvation. In this study, such ambiguity is eliminated by adopting a strategy of covalent trapping of the helical supramolecular polymer to a helical covalent polymer in the crystal lattice. Interestingly, polymerization happened in a single-crystal-to-single-crystal fashion, yielding otherwise challenging helical polymer single crystals. This study discloses a convenient route to access crystals of helical covalent polymers.

Nature has a bias toward helicity from microscopic to macroscopic dimensions; some examples are spiral galaxies, tendrils in plants, Fibonacci spirals in seashells, arrangement of leaves, flower petals, pine cones, and structures of DNA, proteins, and polysaccharides. Natural helical polymers such as DNA, proteins, and polysaccharides, play vital biological functions, such as storage of genetic information, imparting strength by the triple-helical collagen, aiding molecular recognition, stability, specificity, and special functions of helical proteins. This plethora of functions played by helical biopolymers generated great interest in creating both supramolecular (1–14) and covalent helical polymers (CHPs) (15–23). These synthetic helical polymers have applications in chiral chromatography (24), asymmetric catalysis (25, 26), chiral recognition (27), optics (28), controlled release (29), circularly polarized luminescence (30), optical memory (31), spin filtering (32), and biomedical fields (33), among others. As for most applications, polymers are required in their solid form; thus, it is essential to create the property-imparting helical conformation in their solid state. Designing polymers with precise molecular conformation and supramolecular ordering in the solid state is challenging, as solution-synthesized polymers can undergo conformational change upon solvent evaporation. Synthetic CHPs that are characterized in the solid state at atomic resolution by single-crystal X-ray diffraction (SCXRD) are very rare (34–36). Here, we report a regio- and stereospecific single-crystal-to-single-crystal TEAC polymerization of a dipeptide-monomer containing azide and alkene to the corresponding triazoline-linked peptide-polymer having a left-handed helical conformation. This strategy of covalent trapping of the supramolecular helical monomer to a helical polymer in the crystal lattice is of great importance.

Results and Discussion

The orchestration of the reactive groups at a proximal distance in crystals is crucial for any topochemical reaction (37–47). Peptides that form β-stacks are known to adopt a head-to-tail arrangement in a direction perpendicular to the stacking direction (48, 49). This has been exploited for the design of monomers for topochemical azide-alkyne cycloaddition (TAAC) polymerization (36, 47, 50–53). However, the recently developed TEAC reaction is advantageous over the TAAC reaction, as the triazoline units generated can be denitrogenated to aziridine units, thereby offering the possibility of postpolymerization backbone modification (54). Also, since the TEAC reaction generates a new chiral center in the triazoline, the polymerization can be both regiospecific and stereospecific, which could contribute to the helicity of the resultant polymer. Natural and synthetic

Author affiliations: [a]School of Chemistry, Indian Institute of Science Education and Research Thiruvananthapuram, Kerala-695551, India

Author contributions: K.M.S. designed research; R.K. performed research; R.K. and K.M.S. analyzed data; and R.K. and K.M.S. wrote the paper.

The authors declare no competing interest.

This article is a PNAS Direct Submission.

[1]To whom correspondence may be addressed. Email: kms@iisertvm.ac.in.

This article contains supporting information online at http://www.pnas.org/lookup/suppl/doi:10.1073/pnas.2205320119/-/DCSupplemental.

Published July 14, 2022.

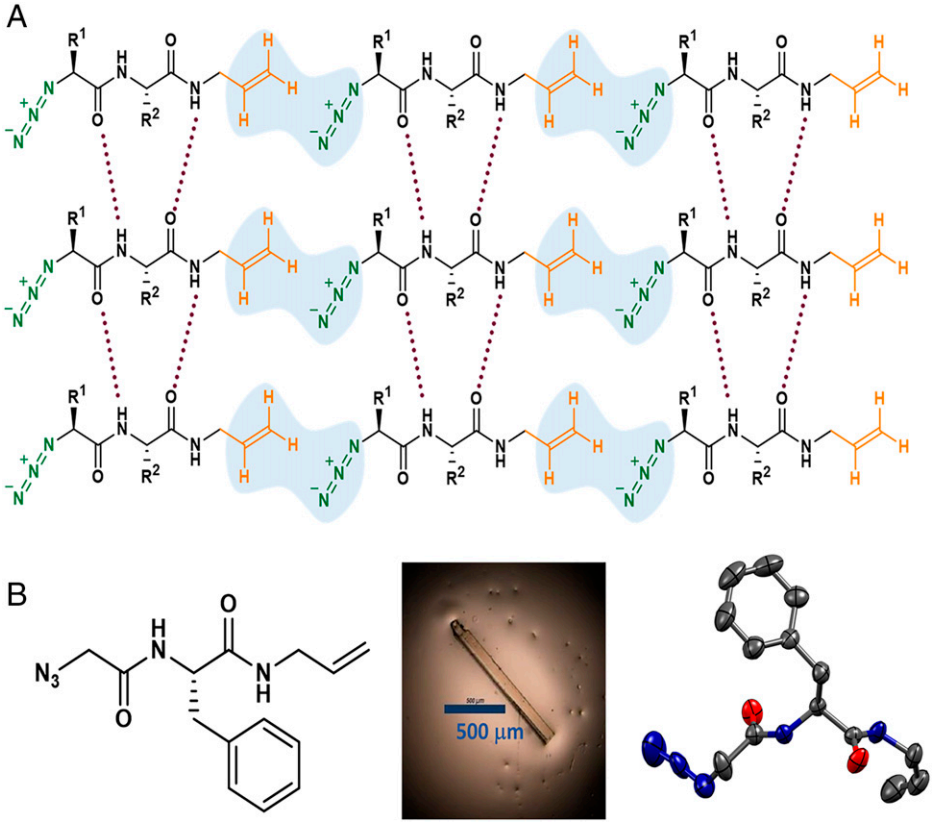

Fig. 1. (*A*) TEAC reaction design. (*B*) Chemical structure, single crystal, and Oak Ridge Thermal Ellipsoid Plot diagram of the monomer 1 (ellipsoids at 50% probability level).

peptides containing phenylalanine are known to have a greater propensity to form β-sheets (48, 55). On the other hand, many β-sheet–dominated natural proteins such as silk and β-keratin are glycine rich (56, 57). Also, many glycine-containing synthetic peptides are known to adopt a β-sheet–like conformation (58). Furthermore, peptides with Gly-Phe units are known to form β-sheet–like packing (36, 59) (Fig. 1*A*), and many natural proteins have Gly-Phe repeats, which are essential for their function (60). Thus, we designed and synthesized the dipeptide 1 as the monomer. We obtained single crystals of monomer 1 as colorless needles (melting point, 132 °C) by slow evaporation of its solution in an equivolume mixture of toluene and acetone (Fig. 1*B* and *SI Appendix*, Fig. S1). The monomer 1 crystallized in the monoclinic space group $P2_1$ with one molecule in the asymmetric unit (Fig. 1*B* and *SI Appendix*, Tables S1 and S2). The peptide backbone adopts a C-shaped conformation (*SI Appendix*, Fig. S2). The azide is disordered over two positions with an occupancy ratio of 0.62:0.38. In both the positions, its β-N makes an azide…oxygen interaction (O…N_β; 3.0 Å) with the carbonyl oxygen (61). The monomer molecules are assembled as β-stacks through *N*-H…O and C-H…O H bonds along the crystallographic direction "a" (Fig. 2*A*). The monomer molecules between adjacent one-dimensional H-bonded stacks are laterally connected through C-H…N and C-H…O H-bonding interactions along the "b" direction. The C-H…N H-bonding between alkenyl hydrogen and γ-N of azide helps in head-to-tail arrangement of the monomer molecules forming a left-handed supramolecular helix along the crystallographic "b" direction (Fig. 2*B*). These supramolecular helical chains are stacked in perpendicular direction through *N*-H…O H-bond, resulting in an exotic helical sheet-like assembly (Fig. 2*C*). The solid-state circular dichroism (CD) spectrum of the monomer 1 shows double-negative maxima at 249 nm and 237 nm with a positive maximum at 228 nm, supporting helical assembly in the crystal (Fig. 2*D*).

The azide and alkene units between adjacent monomer molecules in the supramolecular helices are parallelly arranged. The distances between their termini are 3.6 and 4.8 Å (Fig. 2*B*), suggesting that they are preorganized in a reactive arrangement. We have investigated the reactivity of the monomer 1 single crystals at various temperatures. The crystal did not react at temperatures below 80 °C even after 18 d, as evidenced by ^{1}H NMR spectroscopy. At 80 °C, there was no reaction until the sixth day; on the seventh day, the mixture was only partially soluble in all common solvents such as dichloromethane, $CHCl_3$, MeOH, EtOH, tetrahydrofuran, dimethylformamide, dimethyl sulfoxide, ethyl acetate, and acetone. The ^{1}H NMR spectrum of the soluble fraction showed only the presence of the monomer, suggesting that the polymer formed is entirely insoluble. After the eighth day, the crystals were completely insoluble. At 90 °C, the reaction reached this stage in 6 d. The insoluble material did not melt but decomposed (charred) at 400 °C. We studied the progress of the reaction by analyzing the sample before and after the heating (polymerization) using solid-state infrared (IR), solid-state NMR, powder X-ray diffraction (PXRD), and SCXRD measurements.

The IR spectrum of the monomer showed a prominent peak at 2,099 cm^{-1}, corresponding to the azide stretching. The intensity of this peak was found to be diminished in the case of the heated sample (*SI Appendix*, Fig. S3). The comparison of cross-polarization magic angle spinning (CP-MAS) ^{13}C NMR spectra of the monomer 1 and the heated sample supported the quantitative TEAC polymerization (*SI Appendix*, Figs. S4–S6). A comparison of the PXRD spectrum of the monomer crystals with that of the heated sample showed apparent changes in the

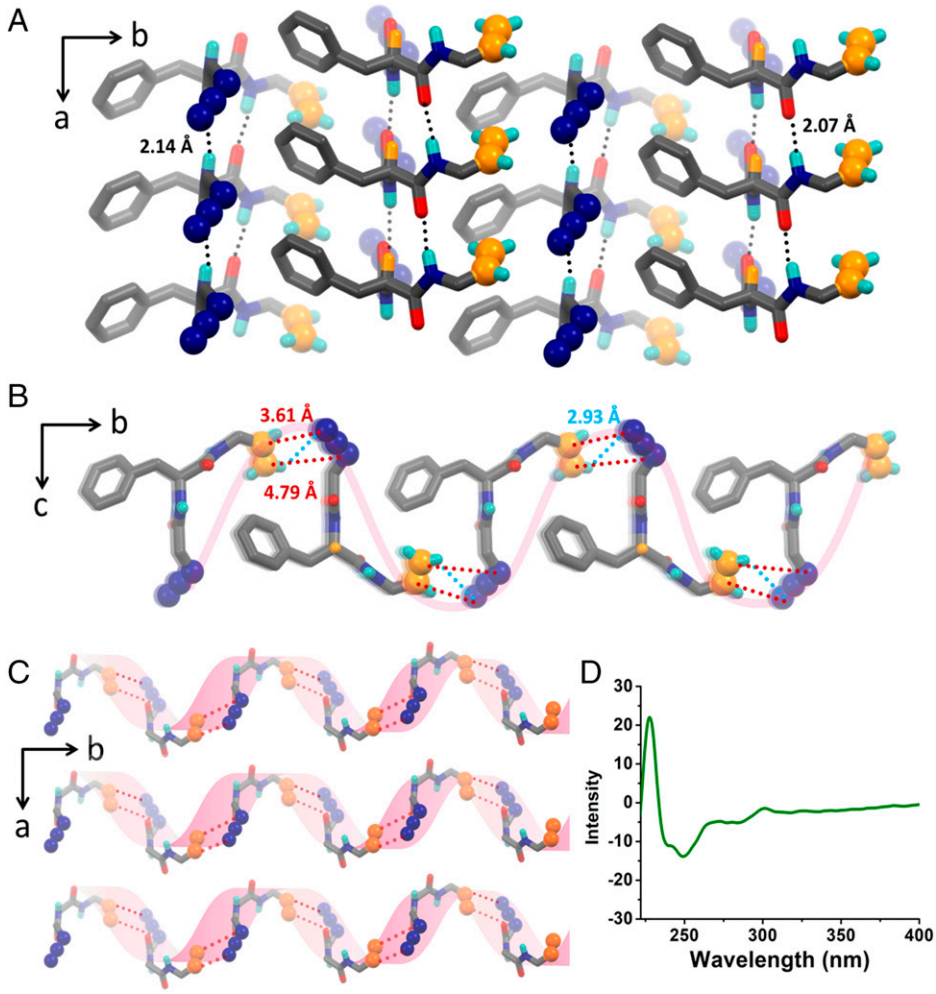

Fig. 2. (*A*) *N*-H…O H-bonded molecules forming a β-sheet–like packing along direction "a." Dotted lines indicate the *N*-H…O bond. (*B*) Head-to-tail arrangement of monomer molecules forming a left-handed supramolecular helix along the "b" direction. The blue dotted line indicates the C-H…N bond. (*C*) View along "c" direction of supramolecular helical-sheet–like assembly; β-sheet and supramolecular helix in mutually perpendicular directions. Azide (blue) and alkene (orange) are highlighted in the ball-and-stick model. H atoms and side chains are hidden for clarity. (*D*) Solid-state CD spectrum of the monomer 1.

diffraction pattern (Fig. 3*D*). Sharp peaks were observed even for the heated (i.e., polymer 1) sample, suggesting that the polymerization reaction occurred, preserving the crystallinity. Furthermore, optical microscopy of the heated sample confirmed that the single crystals remain intact even after polymerization, and polarizing microscopy showed the birefringence characteristic of its crystalline nature (Fig. 3*A*). This suggests that the polymerization reaction is a single-crystal-to-single-crystal transformation.

SCXRD analysis of the heated sample revealed the structure of the polymer. Polymer crystal retained the space group $P2_1$ (*SI Appendix*, Fig. S7 and Tables S1 and S2). The cycloaddition reaction occurred not only in a regiospecific manner but also in a stereospecific fashion to yield 1,4-disubstituted triazoline-linked polymer with the absolute configuration (S) for the newly generated chiral center (Fig. 3*A*). The observed regiospecificity and stereospecificity are similar to those observed for enzyme-mediated reactions. While such specificities in enzymatic reactions arise from the confinement of reactant(s) in chiral enzyme cavities, the confinement of the complementary reactive groups (azide and alkene) in a reactive geometry in the chiral crystal lattice imparts regio- and stereospecificity to this cycloaddition reaction. Since the polymer crystals are insoluble in most common organic solvents, we estimated the molecular weight and degree of polymerization from the single-crystal parameters (34, 62). From the polymer crystal structure, the degree of polymerization and molecular weight (per micrometer) are estimated to be 1,302 and 374 kg mol^{-1}, respectively (*SI Appendix*, Fig. S8). A comparison of the unit cell parameters of the monomer 1 and the polymer 1 suggested increase of the *a* and *c* axes by 2.88% and 1.39%, respectively, but a decrease of the *b* axis by 6.17%. The significant reduction in the *b* axis is due to the closer movement of monomer units in view of the formation of the covalent linkage (triazoline rings) between them.

The polymer chains adopt a helical conformation (Fig. 3*B*) and are laterally connected via H bonding between them (Fig. 3*C*). As expected, the helix exhibits left-handedness with a helical pitch length of 15.35 Å, and two repeating units make a complete turn (Fig. 3*B*). Notably, this left-handedness of the helical polymer 1 contrasts with the right-handedness generally found in the natural helical polymers. The overlay of monomer 1 and polymer 1 crystal structures corroborate the perfectly crystal-engineered TEAC reaction (*SI Appendix*, Fig. S9). It is noteworthy that the polymer structure retains helical-sheet–like architecture with the covalently linked helical chains (Fig. 3*C*). In the "b" direction, the helical backbone runs perpendicular to the β-sheet direction, and such helical chains are connected by intermolecular hydrogen bonds along the "a" direction. The lateral helical assemblies in the "c" direction are glued with the help of weak interactions such as C-H…N H bonding and van

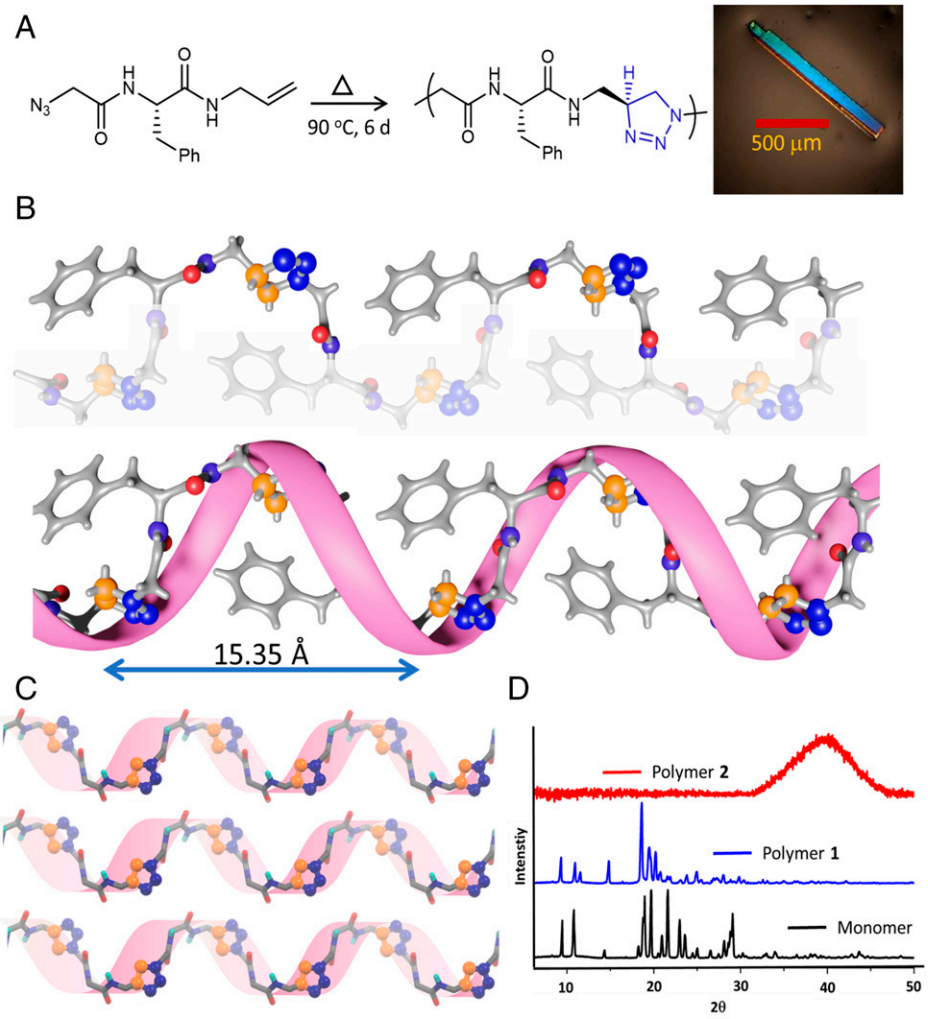

Fig. 3. (*A*) TEAC reaction to yield polymer 1. (*B*) Crystallographic conformation of polymer chains showing helical propagation in the direction "b." (*C*) Helical-sheet–like arrangement of the polymer chains, viewed along the "c" direction. Triazoline rings are highlighted in a ball-and-stick model. H atoms and side chains are hidden for clarity. (*D*) PXRD diffractogram of the monomer, polymer 1, and polymer 2.

der Waals interaction. The solid-state CD signal of the polymer is similar to that of the monomer, which also supports the retention of helical assembly (Fig. 4*A*). This alluring architecture closely resembles the recently reported cross-α amyloid structure, formed via the lateral self-assembly of the α-helical bacterial peptide PSMα3 in a direction perpendicular to the fibril axis (63). It is noteworthy that there has been much interest in synthesizing peptides adopting such modes of assembly (64–66). Furthermore, the hardness and Young's modulus of the polymer 1 crystal were determined to be 1.15 GPa and 10.66 GPa, respectively, indicating the high strength of the CHP assembly (*SI Appendix*, Fig. S11).

Sterically, triazole and triazoline are similar. However, since the TAAC reaction–derived triazole core is aromatic, it is challenging to chemically modify it further. In contrast, the triazoline core can be easily converted to the versatile aziridine core by heating or photo-irradiation (67). In this context, the TEAC reaction could result in triazoline-linked peptides whose linkage can be easily converted into aziridine at will to get a different kind of polypeptide (Fig. 4*B*). In order to explore the possibility of converting the triazoline-linked polymer to aziridine-linked polymer (polymer 2), we have kept a few polymer crystals in silicone oil and heated them. The process was monitored using an optical microscope. At the temperature range of 176 to 210 °C, we observed gas evolution (i.e., bubbles) out of the crystals (Fig. 4*C* and Movie S1), which is attributable to the denitrogenation. Thermogravimetric analysis (TGA) analysis of the polymer 1 crystal evidenced a weight loss of approximately 9% in the temperature range 161 to 205 °C (Fig. 4*D*), which corresponds to the amount of nitrogen (theoretical amount, 9.7%) that can be evolved from the triazoline-linked polymer. Similarly, differential scanning calorimetry (DSC) analysis showed an exothermic peak in the temperature range 175 to 210 °C (Fig. 4*E*) attributable to the exothermic denitrogenation. The CP-MAS ^{13}C NMR showed the shift of peaks corresponding to the carbons present in the triazoline in view of its conversion to aziridine ring (*SI Appendix*, Fig. S10). Similar to the protein denaturation at higher temperatures, the heat-mediated conversion of peptide-based polymer 1 to polymer 2 alters its helical assembly, as revealed by the CD spectroscopy (Fig. 4*A*) and becomes amorphous, as evidenced from its PXRD pattern (Fig. 3*D*). Therefore, at will, one can convert the triazoline core into aziridine core without any chemical reagents, and this simple process can act as a turn-off switch for the crystallinity and helicity.

In conclusion, polymers that display helicity in the solid state are desirable for important applications like chiral stationary phases for high-performance liquid chromatography and catalysis. We have demonstrated a strategy of covalent trapping of supramolecular helical polymers to helical covalent polymer in the crystal by adopting the newly discovered TEAC reaction. The

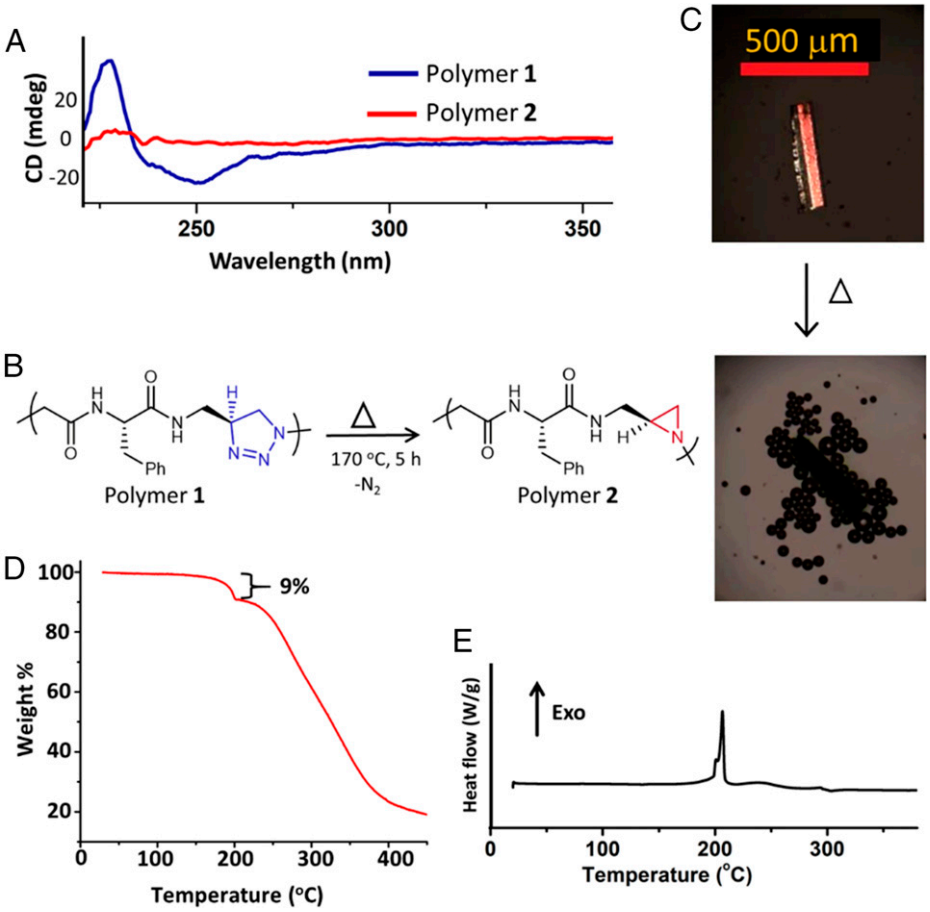

Fig. 4. (*A*) Solid-state CD spectra of polymer 1 and 2. (*B*) Schematic representation of the conversion of polymer 1 to polymer 2. (*C*) Evolution of bubbles from the polymer crystal on heating. (*D*) TGA of the polymer 1 showing the weight loss of 9% due to the loss of nitrogen. (*E*) DSC graph of polymer 1 showing the exothermic peak due to denitrogenation.

designed dipeptide monomer, in its crystals, is organized in head-to-tail fashion, as supramolecular helices, through weak CH…N H-bonding between the azide and alkene units of adjacent molecules. The azide and alkene preorganized in a reactive orientation underwent regiospecific and stereospecific cycloaddition reaction forming triazoline-linked helical polymer in an SCSC manner. The left-handed helical polymer thus obtained is insoluble in most of the common organic solvents and might be a suitable candidate for many solid-state applications. Also, as the triazoline can be denitrogenated to aziridine, the polymer linkage can be easily modified to more a versatile aziridine-linked polymer. This strategy of translating the weakly linked supramolecular helical polymer to a robust CHP may elicit interest in synthesizing many such CHPs via topochemical polymerization.

Materials and Methods

All chemicals were purchased from commercial suppliers and were used without further purification. All solvents were used after distillation. Reactions were monitored by thin-layer chromatography using precoated silica gel plates (60 F_{254}). Thin-layer chromatograms were visualized under ultraviolet light at 254 nm and by heating the plates dipped in the ceric ammonium molybdate staining solution. Column chromatography was carried out using silica gel (230 to 400 mesh) as the stationary phase. ^{1}H NMR and ^{13}C NMR spectra were recorded on a 500 MHz and 125 MHz NMR spectrometer, respectively. Proton chemical shifts (δ) are reported relative to tetramethylsilane (TMS; δ = 0.0) as the internal standard and expressed in parts per million. CP-MAS ^{13}C NMR spectra were recorded on an Avance-III HD-700 MHz (Bruker) Two-Bay NMR spectrometer (16.4 T magnetic field) using a 3.2-mm magic angle spinning (MAS) probe at a sample temperature ~10 °C. Cross-polarization was done to enhance the sensitivity of ^{1}H decoupling. A ^{1}H pulse width of 3 µs was used (contact time is 2 ms). The MAS frequency was set to 10 kHz. ^{13}C chemical shifts were indirectly calibrated to the methylene signal of adamantane (41.1 ppm on the TMS scale). Coupling constants (*J*) are given in Hertz. Protons and carbons were assigned using two-dimensional NMR spectra such as correlated spectroscopy, heteronuclear multiple bond correlation, and nuclear Overhauser effect spectroscopy. IR spectra were recorded using an IR Prestige-21 (Shimadzu) spectrometer.

Melting points were determined by a Stanford Research Systems (EZ-Melt) melting-point apparatus. Specific rotations were recorded on a Rudolph Autopol III automatic polarimeter. Elemental analyses were done on the Elementar vario MICRO cube elemental analyzer. SCXRD data measurements were done via a Bruker-KAPPA APEX II CCD diffractometer with graphite-monochromatized radiation (MoK [Molybdenum Kα] = 0.71073 Å). The X-ray generator was operated at 50 kV and 30 mA. The X-ray data collection was analyzed by the SMART program (Bruker, version 5.631). All the data were corrected for Lorentzian polarization and absorption effects using the SAINTPLUS and SADABS programs (Bruker). SHELXT and SHELXL-2014 were used for structure solution and full-matrix least-squares refinement on F2. Analysis of the crystal structure was done using Mercury 3.9 software. All the hydrogen atoms were placed in geometrically idealized positions and refined in the riding model approximation with C-H equal to 0.95 Å, and with Uiso (H) set to 1.2 Ueq (C). PXRD analysis was done using an X'pert PRO (PANalytics) X-ray diffractometer using Cu as the anode material (Kα1 = 1.540598 Å). DSC analyses were carried out using a DSC Q20 differential scanning calorimeter at a 5 °C/min heating rate. TGA analyses were done using a universal V 4.7A TA instrument at a 5 °C/min heating rate. CD spectra were recorded on a JASCO (J-815) CD spectrometer with a bandwidth of 10 nm and scanning speed of 200 nm/min. Nanoindentation was performed using a nanoindenter (Triboindenter; Hysitron) with force and displacement resolutions if 1 nN and 0.2 nm, respectively. Indentation was done using a three-sided,

pyramidal, Berkovich diamond-indenter sharp tip. We made indentations on the larger face (001) of the polymer 1 crystal. We increased the load up to 1 mN, with the rate of loading and unloading as 0.1 mN/s. The load versus displacement curves were analyzed using the standard Oliver-Pharr method, and reduced elastic modulus was extracted as previously reported (68). Young's modulus and hardness of the samples were also determined as previously reported (68). SDs for Young's modulus and hardness were calculated from several experiments.

Data Availability. Synthesis and characterization of monomer 1, polymer 1, and polymer 2, including DSC, PXRD, SCXRD, IR, and NMR are provided in *SI Appendix*. Movie S1 (Demonstration of N_2 bubbling by heating the crystal kept in immersion oil). The crystal structures of monomer and polymer 1 are available free of charge from the Cambridge Crystallographic Data Centre under reference numbers CCDC-2142306 and CCDC-2142305, respectively (69, 70).

ACKNOWLEDGMENTS. This study was supported in part by a SwarnaJayanti fellowship (DST/SJF/CSA02/2012-13) to K.M.S. by the Department of Science and Technology, Ministry of Science and Technology, Government of India and the research grant (SERB/CRG/000577/2018) from the Science and Engineering Research Board, India. We thank Pratyank Rastogi and Kiran Raphael, Industron Nanotechnology Pvt. Ltd., Trivandrum, India, for helping with nanoindentation experiments.

1. T. Aida, E. W. Meijer, S. I. Stupp, Functional supramolecular polymers. *Science* **335**, 813–817 (2012).
2. X. Chen, Y. He, Y. Kim, M. Lee, Reversible, short α-peptide assembly for controlled capture and selective release of enantiomers. *J. Am. Chem. Soc.* **138**, 5773–5776 (2016).
3. S. Datta, S. Takahashi, S. Yagai, Nanoengineering of curved supramolecular polymers: Toward single-chain mesoscale materials. *Acc. Mater. Res.* **3**, 259–271 (2022).
4. Z. Fernández, B. Fernández, E. Quiñoá, F. Freire, The competitive aggregation pathway of an asymmetric chiral oligo(p-phenyleneethynylene) towards the formation of individual P and M supramolecular helical polymers. *Angew. Chem. Int. Ed.* **60**, 9919–9924 (2021).
5. T. Fukushima *et al.*, Diarylethene-powered light-induced folding of supramolecular polymers. *J. Am. Chem. Soc.* **143**, 5845–5854 (2021).
6. Z. Huang *et al.*, Pulsating tubules from noncovalent macrocycles. *Science* **337**, 1521–1526 (2012).
7. J. Kang *et al.*, A rational strategy for the realization of chain-growth supramolecular polymerization. *Science* **347**, 646–651 (2015).
8. Y. Kitamoto *et al.*, One-shot preparation of topologically chimeric nanofibers via a gradient supramolecular copolymerization. *Nat. Commun.* **10**, 4578 (2019).
9. K. Salikolimi *et al.*, Helical supramolecular polymers with rationally designed binding sites for chiral guest recognition. *Nat. Commun.* **11**, 2311 (2020).
10. S. Shin *et al.*, Supramolecular switching between flat sheets and helical tubules triggered by coordination interaction. *J. Am. Chem. Soc.* **135**, 2156–2159 (2013).
11. M. L. Ślęczkowski, M. F. J. Mabesoone, P. Ślęczkowski, A. R. A. Palmans, E. W. Meijer, Competition between chiral solvents and chiral monomers in the helical bias of supramolecular polymers. *Nat. Chem.* **13**, 200–207 (2021).
12. N. J. V. Zee, M. F. J. Mabesoone, B. Adelizzi, A. R. A. Palmans, E. W. Meijer, Biasing the screw-sense of supramolecular coassemblies featuring multiple helical states. *J. Am. Chem. Soc.* **142**, 20191–20200 (2020).
13. M. Yamauchi, T. Ohba, T. Karatsu, S. Yagai, Photoreactive helical nanoaggregates exhibiting morphology transition on thermal reconstruction. *Nat. Commun.* **6**, 8936 (2015).
14. E. Yashima *et al.*, Supramolecular helical systems: Helical assemblies of small molecules, foldamers, and polymers with chiral amplification and their functions. *Chem. Rev.* **116**, 13752–13990 (2016).
15. J. J. L. M. Cornelissen *et al.*, β-helical polymers from isocyanopeptides. *Science* **293**, 676–680 (2001).
16. J. Eglil, C. Esposito, M. Müri, S. Riniker, H. Wennemers, Influence of lipidation on the folding and stability of collagen triple helices–An experimental and theoretical study. *J. Am. Chem. Soc.* **143**, 5937–5942 (2021).
17. Z. Fernández, B. Fernández, E. Quiñoá, F. Freire, Merging supramolecular and covalent helical polymers: Four helices within a single scaffold. *J. Am. Chem. Soc.* **143**, 20962–20969 (2021).
18. T. Nakano, Y. Okamoto, Synthetic helical polymers: Conformation and function. *Chem. Rev.* **101**, 4013–4038 (2001).
19. R. Rodríguez, E. Quiñoá, R. Riguera, F. Freire, Architecture of chiral poly(phenylacetylene)s: From compressed/highly dynamic to stretched/quasi-static helices. *J. Am. Chem. Soc.* **138**, 9620–9628 (2016).
20. R. Rodríguez, E. Suárez-Picado, E. Quiñoá, R. Riguera, F. A. Freire, Stimuli-responsive macromolecular gear: Interlocking dynamic helical polymers with foldamers. *Angew. Chem. Int. Ed.* **59**, 8616–8622 (2020).
21. E. Yashima, K. Maeda, Helical polymers with dynamic and static macromolecular helicity memory: The power of helicity memory for helical polymer synthesis and applications. *Bull. Chem. Soc. Jpn.* **94**, 2637–2661 (2021).
22. E. Yashima, K. Maeda, H. Iida, Y. Furusho, K. Nagai, Helical polymers: Synthesis, structures, and functions. *Chem. Rev.* **109**, 6102–6211 (2009).
23. W. Zheng, T. Ikai, E. Yashima, Synthesis of single-handed helical spiro-conjugated ladder polymers through quantitative and chemoselective cyclizations. *Angew. Chem. Int. Ed.* **60**, 11294–11299 (2021).
24. J. Shen, Y. Okamoto, Efficient separation of enantiomers using stereoregular chiral polymers. *Chem. Rev.* **116**, 1094–1138 (2016).
25. T. Ikai *et al.*, Emergence of highly enantioselective catalytic activity in a helical polymer mediated by deracemization of racemic pendants. *J. Am. Chem. Soc.* **143**, 12725–12735 (2021).
26. S. Juliá, J. Masana, J. C. Vega, "Synthetic enzymes". Highly stereoselective epoxidation of chalcone in a triphasic toluene-water-poly[(S)-alanine] system. *Angew. Chem. Int. Ed. Engl.* **19**, 929–931 (1980).
27. T. Ikai *et al.*, Helix-sense-selective encapsulation of helical poly(lactic acid)s within a helical cavity of syndiotactic poly(methyl methacrylate) with helicity memory. *J. Am. Chem. Soc.* **142**, 21913–21925 (2020).
28. P. Wang *et al.*, Insights into magneto-optics of helical conjugated polymers. *J. Am. Chem. Soc.* **140**, 6501–6508 (2018).
29. Y. Zhang, J. Deng, Chiral helical polymer materials derived from achiral monomers and their chiral applications. *Polym. Chem.* **11**, 5407–5423 (2020).
30. J. Li, G. B. Schuster, K.-S. Cheon, M. M. Green, J. V. Selinger, Switching a helical polymer between mirror images using circularly polarized light. *J. Am. Chem. Soc.* **122**, 2603–2612 (2000).
31. K. Maeda *et al.*, Helix-sense-selective synthesis of right- and left-handed helical luminescent poly(diphenylacetylene)s with memory of the macromolecular helicity and their helical structures. *J. Am. Chem. Soc.* **142**, 7668–7682 (2020).
32. S. Mishra *et al.*, Spin filtering along chiral polymers. *Angew. Chem. Int. Ed.* **59**, 14671–14676 (2020).
33. T. Leigh, P. Fernandez-Trillo, Helical polymers for biological and medical applications. *Nat. Rev. Chem.* **4**, 291–310 (2020).
34. Y. Hu *et al.*, Single crystals of mechanically entwined helical covalent polymers. *Nat. Chem.* **13**, 660–665 (2021).
35. Y. Wang *et al.*, Double helical conformation and extreme rigidity in a rodlike polyelectrolyte. *Nat. Commun.* **10**, 801 (2019).
36. K. Hema, K. M. Sureshan, β-Sheet to helical-sheet evolution induced by topochemical polymerization: Cross-α-amyloid-like packing in a pseudoprotein with gly-phe-gly repeats. *Angew. Chem. Int. Ed.* **59**, 8854–8859 (2020).
37. K. Biradha, R. Santra, Crystal engineering of topochemical solid state reactions. *Chem. Soc. Rev.* **42**, 950–967 (2013).
38. A. Matsumoto, T. Odani, K. Sada, M. Miyata, K. Tashiro, Intercalation of alkylamines into an organic polymer crystal. *Nature* **405**, 328–330 (2000).
39. M. J. Kory *et al.*, Gram-scale synthesis of two-dimensional polymer crystals and their structure analysis by X-ray diffraction. *Nat. Chem.* **6**, 779–784 (2014).
40. P. Kissel, D. J. Murray, W. J. Wulftange, V. J. Catalano, B. T. King, A nanoporous two-dimensional polymer by single-crystal-to-single-crystal photopolymerization. *Nat. Chem.* **6**, 774–778 (2014).
41. R. S. Jordan *et al.*, Synthesis of graphene nanoribbons via the topochemical polymerization and subsequent aromatization of a diacetylene precursor. *Chem* **1**, 78–90 (2016).
42. P. Zhang *et al.*, Distance-selected topochemical dehydro-Diels–Alder reaction of 1,4-diphenylbutadiyne toward crystalline graphitic nanoribbons. *J. Am. Chem. Soc.* **142**, 17662–17669 (2020).
43. L. Dou *et al.*, Single-crystal linear polymers through visible light-triggered topochemical quantitative polymerization. *Science* **343**, 272–277 (2014).
44. F. Hu *et al.*, Highly efficient preparation of single-layer two-dimensional polymer obtained from single-crystal to single-crystal synthesis. *J. Am. Chem. Soc.* **143**, 5636–5642 (2021).
45. S. P. Yelgaonkar, G. Campillo-Alvarado, L. R. MacGillivray, Phototriggered guest release from a nonporous organic crystal: Remarkable single-crystal-to-single-crystal transformation of a binary cocrystal solvate to a ternary cocrystal. *J. Am. Chem. Soc.* **142**, 20772–20777 (2020).
46. I. E. Claassens, L. J. Barbour, D. A. Haynes, A multistimulus responsive porous coordination polymer: Temperature-mediated control of solid-state [2 + 2] cycloaddition. *J. Am. Chem. Soc.* **141**, 11425–11429 (2019).
47. K. Hema, K. M. Sureshan, Topochemical azide–alkyne cycloaddition reaction. *Acc. Chem. Res.* **52**, 3149–3163 (2019).
48. S. Bera, S. Mondal, S. Rencus-Lazar, E. Gazit, Organization of amino acids into layered supramolecular secondary structures. *Acc. Chem. Res.* **51**, 2187–2197 (2018).
49. C. Yuan *et al.*, Hierarchically oriented organization in supramolecular peptide crystals. *Nat. Rev. Chem.* **3**, 567–588 (2019).
50. V. Athiyarath, M. C. Madhusudhanan, S. Kunnikuruvan, K. M. Sureshan, Secondary structure tuning of a pseudoprotein between β-meander and α-helical forms in the solid-state. *Angew. Chem. Int. Ed.* **61**, e202113129 (2022).
51. B. P. Krishnan, R. Rai, A. Asokan, K. M. Sureshan, Crystal-to-crystal synthesis of triazole-linked pseudo-proteins via topochemical azide–alkyne cycloaddition reaction. *J. Am. Chem. Soc.* **138**, 14824–14827 (2016).
52. R. Mohanrao, K. Hema, K. M. Sureshan, Topochemical synthesis of different polymorphs of polymers as a paradigm for tuning properties of polymers. *Nat. Commun.* **11**, 865 (2020).
53. R. Rai, B. P. Krishnan, K. M. Sureshan, Chirality-controlled spontaneous twisting of crystals due to thermal topochemical reaction. *Proc. Natl. Acad. Sci. U.S.A.* **115**, 2896–2901 (2018).
54. R. Khazeber, K. M. Sureshan, Topochemical ene–azide cycloaddition reaction. *Angew. Chem. Int. Ed.* **60**, 24875–24881 (2021).
55. C. K. Smith, L. Regan, Guidelines for protein design: The energetics of β-sheet side chain interactions. *Science* **270**, 980–982 (1995).
56. M. Xu, R. V. Lewis, Structure of a protein superfiber: Spider dragline silk. *Proc. Natl. Acad. Sci. U.S.A.* **87**, 7120–7124 (1990).
57. R. D. B. Fraser, D. A. D. Parry, The role of β-sheets in the structure and assembly of keratins. *Biophys. Rev.* **1**, 27 (2009).
58. P.-N. Cheng, J. D. Pham, J. S. Nowick, The supramolecular chemistry of β-sheets. *J. Am. Chem. Soc.* **135**, 5477–5492 (2013).
59. H. Wang *et al.*, Anti-degradation of a recombinant complex protein by incorporation in small molecular hydrogels. *Chem. Commun.* **47**, 955–957 (2011).
60. W. Yan, E. A. Craig, The glycine-phenylalanine-rich region determines the specificity of the yeast Hsp40 Sis1. *Mol. Cell. Biol.* **19**, 7751–7758 (1999).
61. M. C. Madhusudhanan, H. Balan, D. B. Werz, K. M. Sureshan, Azide···oxygen interaction: A crystal engineering tool for conformational locking. *Angew. Chem. Int. Ed.* **60**, 22797–22803 (2021).
62. Q.-H. Guo *et al.*, Single-crystal polycationic polymers obtained by single-crystal-to-single-crystal photopolymerization. *J. Am. Chem. Soc.* **142**, 6180–6187 (2020).

63. E. Tayeb-Fligelman *et al.*, The cytotoxic staphylococcus aureus PSMα3 reveals a cross-α amyloid-like fibril. *Science* **355**, 831–833 (2017).
64. S.-Q. Zhang *et al.*, Designed peptides that assemble into cross-α amyloid-like structures. *Nat. Chem. Biol.* **14**, 870–875 (2018).
65. S. Bera *et al.*, Rigid helical-like assemblies from a self-aggregating tripeptide. *Nat. Mater.* **18**, 503–509 (2019).
66. S. Mondal *et al.*, Transition of metastable cross-α crystals into cross-β fibrils by β-turn flipping. *J. Am. Chem. Soc.* **141**, 363–369 (2019).
67. D. de Loera, A. Stopin, M. A. Garcia-Garibay, Photoinduced and thermal denitrogenation of bulky triazoline crystals: Insights into solid-to-solid transformation. *J. Am. Chem. Soc.* **135**, 6626–6632 (2013).
68. U. Ramamurty, J. I. Jang, Nanoindentation for probing the mechanical behavior of molecular crystals–A review of the technique and how to use it. *CrystEngComm* **16**, 12–23 (2014).
69. R. Khazebera, K. M. Sureshan, Single-crystal-to-single-crystal translation of a helical supramolecular polymer to a helical covalent polymer. Cambridge Crystallographic Data Centre. https://www.ccdc.cam.ac.uk/structures/Search?Ccdcid=CCDC-2142306&DatabaseToSearch=Published. Deposited 15 January 2022.
70. R. Khazebera, K. M. Sureshan, Single-crystal-to-single-crystal translation of a helical supramolecular polymer to a helical covalent polymer. Cambridge Crystallographic Data Centre. https://www.ccdc.cam.ac.uk/structures/Search?Ccdcid=CCDC-2142305&DatabaseToSearch=Published. Deposited 15 January 2022.